SPHCOR. The A^* data for μR from 0·0 to 2·5 are taken from Dwiggins (1975) and the values of $(1/A^*)(dA^*/d\mu R)$ are given in Table 1. $\bar{T}$ values are retrieved by multiplying $(1/A^*)(dA^*/d\mu R)$ by R at the appropriate values of μR and θ.

The accuracy of the table of A^* values (Dwiggins, 1975) is claimed to be 0·05%. We have compared the values of A^* of Dwiggins and $\bar{T}$ calculated by the present method with values given by a Gaussian-grid integration program of unknown accuracy obtained from Cromer (1977). For example, for a value of $\mu R = 1{\cdot}0$ we find relative discrepancies in the A^* values of 0·06% ($\theta = 0°$) and 0·1% ($\theta = 90°$), whereas those in the $\bar{T}$ values are 0·03% ($\theta = 0°$) and 0·05% ($\theta = 90°$). We conclude that the accuracy of our $\bar{T}$ table is about 0·05%.

This work was supported by the Swiss National Science Foundation under project No. 2.173-0.74.

APPENDIX

1. We desire the derivative dy/dx at $x = 0$ for a fourth-order polynomial passing through the points

$$(-2x,y_{2-})(-x,y_-)(0,y_0)(x,y_+)(2x,y_{2+}).$$

Thus we fix

$$y = Ax^4 + Bx^3 + Cx^2 + Dx + E \qquad (1)$$

and

$$\frac{dy}{dx} = 4Ax^3 + 3Bx^2 + 2Cx + D$$

$$\left(\frac{dy}{dx}\right)_{x=0} = D$$

Substituting for the values of the points in (1), we obtain

$$y_{2-} = 16Ax^4 - 8Bx^3 + 4Cx^2 - 2Dx + E$$

$$y_- = Ax^4 - Bx^3 + Cx^2 - Dx + E$$

$$y_0 = E$$

$$y_+ = Ax^4 + Bx^3 + Cx^2 + Dx + E$$

$$y_{2+} = 16Ax^4 + 8Bx^3 + 4Cx^2 + 2Dx + E.$$

Solving for D, we find

$$D = \left(\frac{dy}{dx}\right)_{x=0} = \frac{y_{2-} - 8y_- + 8y_+ - y_{2+}}{12x}.$$

2. We desire $(dy/dx)_{x=0}$ for a fourth-order polynomial (1) passing through the points $(-x,y_-)(0,y_0)(x,y_+)$-$(2x,y_{2+})$ and having $(dy/dx)_{-x} = 1{\cdot}5$. Thus we obtain

$$y_- = Ax^4 - Bx^3 + Cx^2 - Dx + E$$

$$y_0 = E$$

$$y_+ = Ax^4 + Bx^3 + Cx^2 + Dx + E$$

$$y_{2+} = 16Ax^4 + 8Bx^3 + 4Cx^2 + 2Dx + E$$

$$1.5 = -4Ax^3 + 3Bx^2 - 2Cx + D.$$

Solving for D we find

$$D = \left(\frac{dy}{dx}\right)_{x=0} = \frac{1}{18x}(-17y_- + 9y_0 + 9y_+ - y_{2+} - 9x).$$

References

BECKER, P. J. & COPPENS, P. (1974). *Acta Cryst.* A**30**, 129–147.

COPPENS, P. & HAMILTON, W. C. (1970). *Acta Cryst.* A**26**, 71–83.

CROMER, D. (1977). Private communication.

DWIGGINS, C. W. (1975). *Acta Cryst.* A**31**, 395–396.

Acta Cryst. (1978). A**34**, 491–497

The Crystal Structure of Ganophyllite, a Complex Manganese Aluminosilicate. I. Polytypism and Structural Variation

BY D. A. JEFFERSON

Edward Davies Chemical Laboratories, University College of Wales, Aberystwyth SY23 1NE, Wales

(*Received* 5 *December* 1977; *accepted* 7 *January* 1978)

The reciprocal-lattice geometry of ganophyllite has been investigated by X-ray diffraction, two distinct variants being noted. These structures, comprising a monoclinic form and a hitherto unreported triclinic variant, can both be interpreted in terms of structural columns which can be stacked in varying sequences along either of the {011} planes. Diffracted intensities from models of this type for both variants give good agreement with the distinctive pattern of intensities actually observed. With the structural column concept, it is also possible to explain instances of two-dimensionally disordered intergrowths of these structures.

Introduction

The complex manganese silicate ganophyllite was first described by Hamberg (1890) from an occurrence in Sweden. The mineral has subsequently been identified in various locations, and apparent ambiguities in optical properties of specimens from different sources led Smith & Frondel (1968) to undertake a detailed single-crystal X-ray examination. This revealed that samples of so-called ganophyllite frequently consisted of two distinct minerals, the more common of which was referred to as true ganophyllite, the less common as bannisterite. Cell dimensions of both minerals are listed in Table 1, each having a relatively large monoclinic cell and being assigned to space group $A2/a$ such that, in common with other layered silicates, the principal cleavage could be assigned as {001}. No complete structural investigation was reported but it was noted that the composition of these minerals could not be reconciled with any existing group of silicates, and it was suggested that both showed strong similarities to the complex, iron-rich silicate stilpnomelane, particularly as regards the separation of (00l) reciprocal-lattice maxima, and the presence of strong reciprocal-lattice rows parallel to $\mathbf{z}^*$.

The structure determination of stilpnomelane (Eggleton & Bailey, 1965; Eggleton, 1972) revealed it to be a true layered silicate, albeit of a hybrid type similar to zussmanite (Lopes-Vieira & Zussman, 1969). In stilpnomelane Si–O tetrahedral networks are of limited extent, unlike their infinite counterparts in the micas, and are linked by further SiO_4 tetrahedra which also bond one complete structural layer to another. The interlayer spacing so produced corresponds closely with the (004) d spacing in ganophyllite, but at the outset of the present investigation, it became evident that no simple modification of the stilpnomelane structure would fit the unit cell of ganophyllite. Furthermore, an examination of the reciprocal lattice of the latter indicated that similarities in intensity variations to those observed in stilpnomelane were only apparent in certain directions: in general, reciprocal lattices of the two minerals differed widely. Ganophyllite also displayed many non-space-group systematic absences, a feature not noted in stilpnomelane, and evidence was found indicating the existence of at least two crystallographic forms. In contrast to the polytypes of stilpnomelane (Crawford, Jefferson & Thomas, 1977) these were not the result of varying the stacking sequence of layers parallel to (001). Consequently, it was necessary to elucidate the exact nature of the non-space-group absences and intergrowths of the various crystallographic variants of ganophyllite before proceeding with a complete structure determination, in order to reduce the large number of parameters which had to be evaluated. The results of this study are reported below, with the determination of the asymmetric-unit contents forming a subsequent publication.

Table 1. *Accepted cell constants for the minerals ganophyllite and bannisterite* (*Smith & Frondel*, 1968)

	Ganophyllite	Bannisterite
a	16·60 ± 0·05 Å	22·20 ± 0·07 Å
b	27·04 ± 0·08 Å	16·32 ± 0·05 Å
c	50·34 ± 0·15 Å	24·70 ± 0·08 Å
β	94°10′ ± 10′	94°20′ ± 10′
Space group	$A2/a$	$A2/a$

Experimental

The sample of ganophyllite used in this investigation was of Swedish origin,† kindly supplied by Dr A. C. Bishop of the British Museum. Several single crystals were obtained for X-ray diffraction studies, and were examined by the precession method with Ni-filtered Cu radiation. Precession angles of 25 or 30° were utilized, with, in most cases, the precession axis normal to (100) of the monoclinic unit cell. Reciprocal-lattice sections (hkl) with $h = 0, 1, 2, 3$ were recorded for all crystals, with, in one case, an additional examination of sections with $k = 0, 1, 2$.

Variation of intensity in reciprocal space

The overall distribution of intensity observed in the reciprocal lattice of ganophyllite was quite distinctive, differing radically from that in stilpnomelane. Schematic illustrations of the reciprocal lattices of both minerals projected down $\mathbf{z}^*$ are shown in Fig. 1, and it is apparent that the pseudo-trigonal symmetry of stilpnomelane is not shared by ganophyllite. In fact, the only close similarity exists if the ($h0l$) section of ganophyllite is compared with the (hhl) section of stil-

† British Museum Catalogue No. BM 80037.

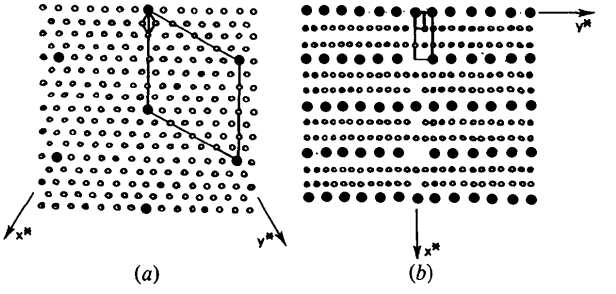

Fig. 1. Overall distribution of intensity in reciprocal space shown by (*a*) stilpnomelane (*b*) ganophyllite, projected down $\mathbf{z}^*$ in each case. Reciprocal-lattice rows which are stronger than average are denoted by the filled circles and unit meshes corresponding to the true lattice and the strong spots only are indicated.

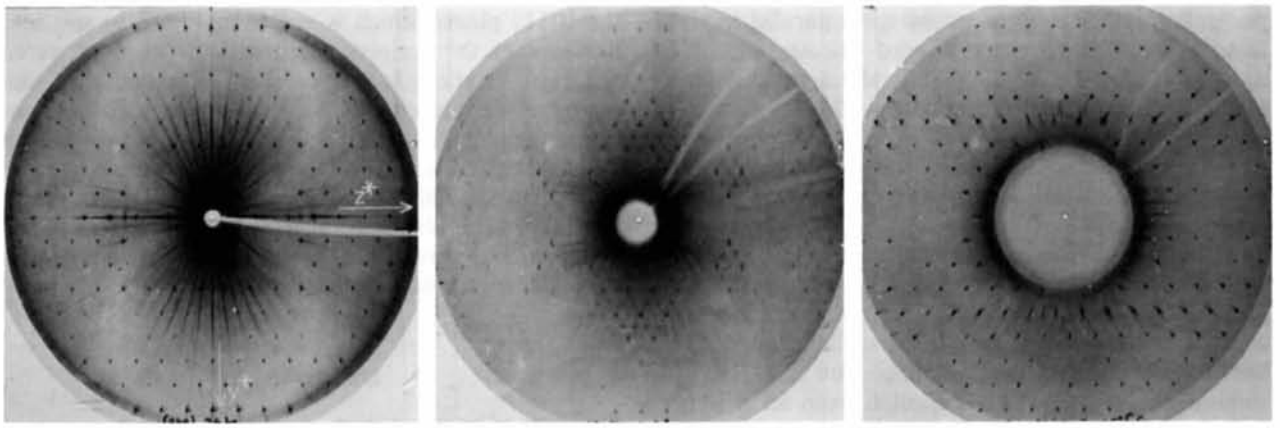

(*a*) (*b*) (*c*)

Fig. 2. X-ray precession photographs of a ganophyllite crystal showing overall monoclinic symmetry (*a*) (0*kl*) section, (*b*) (1*kl*) section, (*c*) (3*kl*) section ($\bar{\mu} = 30°$, Ni-filtered Cu radiation).

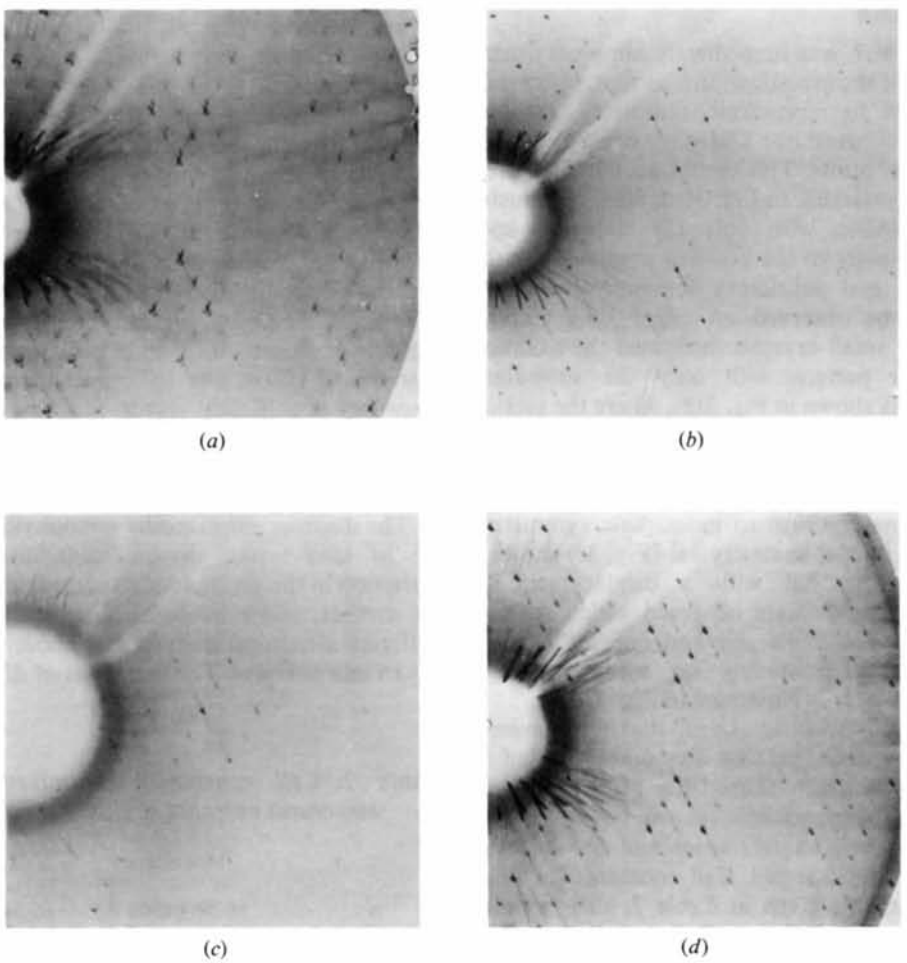

(*a*) (*b*)

(*c*) (*d*)

Fig. 3. Enlargements of X-ray precession photographs of ganophyllite crystals showing different structural variants: (*a*) monoclinic and twinned triclinic, (1*kl*) section; (*b*) triclinic, (1*kl*) section; (*c*) triclinic, (2*kl*) section; (*d*) monoclinic and untwinned triclinic, (1*kl*) section ($\bar{\mu} = 30°$, Ni-filtered Cu radiation).

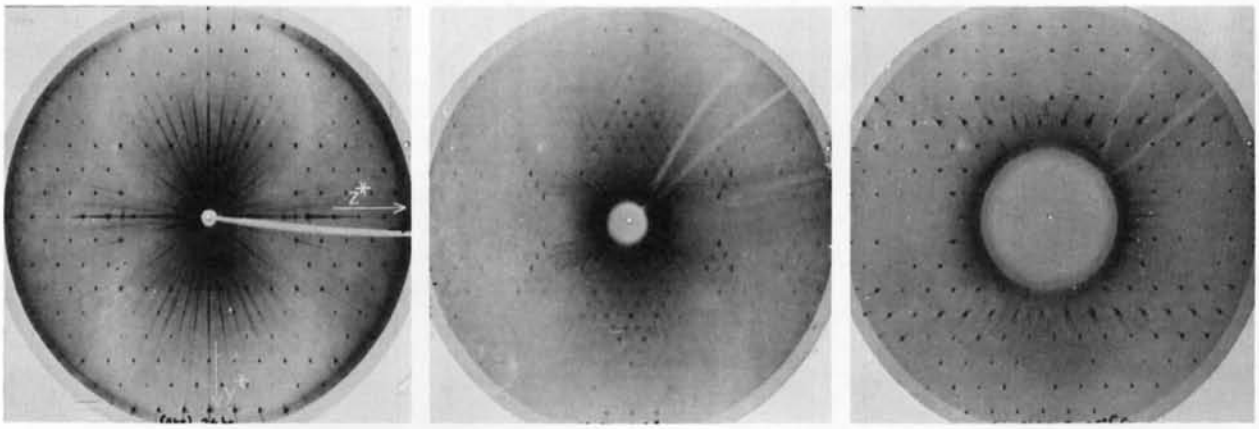

(*a*) (*b*) (*c*)

Fig. 2. X-ray precession photographs of a ganophyllite crystal showing overall monoclinic symmetry (*a*) (0*kl*) section, (*b*) (1*kl*) section, (*c*) (3*kl*) section ($\bar{\mu} = 30°$, Ni-filtered Cu radiation).

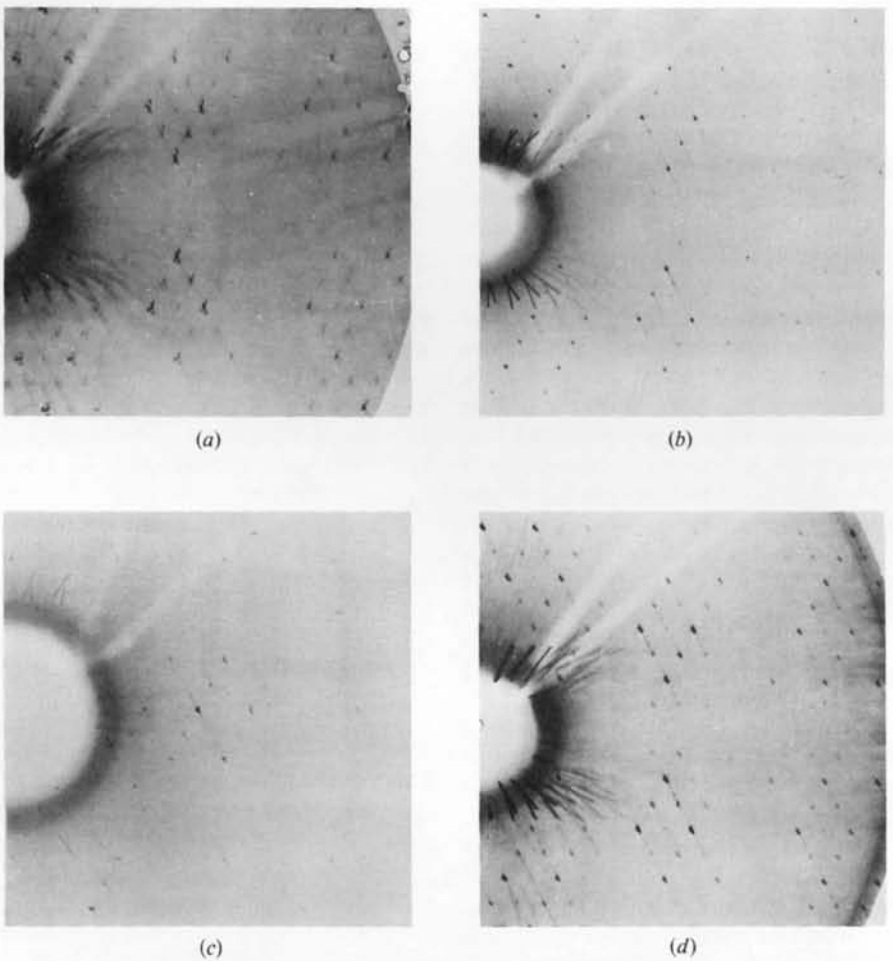

(*a*) (*b*)

(*c*) (*d*)

Fig. 3. Enlargements of X-ray precession photographs of ganophyllite crystals showing different structural variants: (*a*) monoclinic and twinned triclinic, (1*kl*) section; (*b*) triclinic, (1*kl*) section; (*c*) triclinic, (2*kl*) section; (*d*) monoclinic and untwinned triclinic, (1*kl*) section ($\bar{\mu} = 30°$, Ni-filtered Cu radiation).

pnomelane, when rows of strong spots parallel to **z*** (a feature common to most layered silicates) occur in approximately the same place, although the intermediate, weak rows do not coincide. In terms of indices, strong rows of spots occur in stilpnomelane when $h = 4n_1$, $k = 4n_2$ and $h + k = 12n_3$, whereas in ganophyllite all maxima with $h = 3n$ are stronger than the average.

Reciprocal-lattice sections with $h = 3n$ in ganophyllite were also characterized by the presence of pronounced, non-space-group systematic absences. In crystals corresponding to the monoclinic unit cell of Smith & Frondel (1968), sections with $h = 3n \pm 1$ showed only the absences expected from an *A* lattice and an *a* glide plane: sections with $h = 3n$, however, showed the additional absences: $h = 6n$, reflections occurred only if $k + l = 4n$, and $h = 6n + 3$, if $k + l = 4n + 2$. This is illustrated in Fig. 2, which shows $(0kl)$, $(1kl)$ and $(3kl)$ sections.

Structural variation

One feature which was immediately apparent during the early stages of the investigation was that, in crystals which conformed to monoclinic symmetry, maxima with $h = 3n \pm 1$ were not single maxima, but were clusters of smaller spots. This can be seen in Fig. 2(*b*), which is shown, enlarged, in Fig. 3(*a*). Here the cluster is clearly discernible, with only the strongest spot corresponding exactly to the position predicted for the monoclinic cell, and subsidiary maxima with some diffuseness can be observed on either side. Careful selection of very small crystals facilitated the isolation of a diffraction pattern with only the subsidiary maxima visible, as shown in Fig. 3(*b*), where the section and quadrant in reciprocal space are identical with that of Fig. 3(*a*), although the arrangement of maxima is very different. In Fig. 3(*b*) neither positions nor intensities of spots conform to monoclinic symmetry: the $(2kl)$ section for the same crystal (Fig. 3*c*) shows a similar arrangement, but with a displacement of maxima. Other crystals were observed which showed maxima for the monoclinic cell and one set only of subsidiary maxima, producing an overall triclinic symmetry. Such a case is illustrated in Fig. 3(*d*).

Measurement of the positions of maxima showing triclinic symmetry indicated that they corresponded to a triclinic unit cell which shared the [100] axis and $(00l)$ planes with the monoclinic variant, but with [010] and [001] axes approximately twice and one-half the values for the monoclinic cell. Cell constants for both structural variants are given in Table 2, their mutual orientations being plotted on a stereographic projection in Fig. 4. Diffraction evidence therefore pointed to a complex intergrowth of one monoclinic and two twin-related triclinic variants, with some considerable disorder present, as indicated by diffuse streaking normal to the {011} planes which is visible in Fig. 3(*b*) and (*c*). Sections of the reciprocal lattice with $h = 3n$ were, however, identical for all crystals, irrespective of the nature of the intergrowth, and maxima on such sections were completely sharp. Whereas non-space-group systematic absences were confined to those levels in monoclinic crystals, the triclinic variants also appeared to exhibit such absences on $h = 3n \pm 1$ sections. This latter feature provided a clue to the elucidation of the arrangement within the triclinic form.

Discussion

Problems of interpretation

The structural variation and disorder observed in ganophyllite provided further evidence that the structure differed considerably from that in stilpnomelane, and could also be used to simplify greatly the final structure determination. With the type of intergrowth observed, however, the principal difficulty was one of interpretation. Whereas, in layered silicates such as mica, polytypic intergrowths are of frequent occurrence, with (001) as the fault plane and a diffuse streaking of some or all reciprocal-lattice maxima parallel to **z***, the pattern in ganophyllite is more complex, with (011) or $(01\bar{1})$ as fault planes, and a streaking of maxima in directions normal to those planes. Effectively, therefore, the problem is a two-dimensional, rather than a one-dimensional, disorder, with a possibility that diffuse scattering can occur in planes of reciprocal space. If the structure of ganophyllite is likened to a layer structure, with the layers parallel to (001), the structural variation occurs not because of different layer stacking sequences, but because of a variation in the arrangement of individual structural units within each layer, a phenomenon which has not previously been observed in layered silicates.

The disorder exhibited by ganophyllite crystals could be of two types: displacement disorder, involving variation in the position of structural units from one cell to another, and substitutional, where the possibility of different structural units in neighbouring cells must be taken into account. The two types of disorder are not as

Table 2. *Cell constants determined for the two structural variants of ganophyllite observed*

	Monoclinic	Triclinic
a	16·54 ± 0·05 Å	16·54 ± 0·05 Å
b	27·01 ± 0·02 Å	54·30 ± 0·09 Å
c	50·25 ± 0·05 Å	28·52 ± 0·08 Å
α		127°28′ ± 16′
β	94°37′ ± 12′	94°04′ ± 12′
γ		95°50′ ± 12′
Space group	*A*2/*a*	$P\bar{1}$ or *P*1

readily distinguishable as might at first seem apparent, but as the substitutional type is, in general, more difficult to treat analytically, and because a suitable mechanism for the observed disorder could be evolved assuming displacements only, the displacement model was adopted for ganophyllite. A further decisive factor was that true substitutional disorder usually affects all maxima in reciprocal space, a situation which did not apply in the case of ganophyllite.

With a displacement model, two types of analysis can be applied. The simplest, and one which is mathematically more elegant, is to consider the stacking sequences of slabs of structure in a direction normal to one of the fault planes only: the problem then becomes one-dimensional and can be treated with the concept of the average Patterson function (Cochran & Howells, 1954), which is subsequently Fourier-transformed to produce the intensity distribution. With this method, the nature of disordered monoclinic/triclinic intergrowths in wollastonite (Jefferson & Bown, 1973) and rhombohedral/triclinic intergrowths in zussmanite (Jefferson, 1976) have been determined, and relative reciprocal-lattice intensities for the various polytypes predicted. This type of analysis was initially applied to ganophyllite, producing models which explained the observed intensity variations, but in a case where two sets of fault planes can operate simultaneously it is of necessity somewhat artificial. In particular, a case such as that shown in Fig. 3(*a*), where both monoclinic and the twinned triclinic forms are present, could not be treated by a one-dimensional approach, and to provide an acceptable model, a more basic analysis was applied, based on structural columns.

Structural columns

In any basic analysis, it is necessary to abandon the concept of structural slabs running through the crystal and to consider instead structural columns, with the direction of the column parallel to the [100] axis and faces parallel to the fault planes in the lattice. One such column, outlined against the boundaries of the monoclinic cell, is shown in Fig. 5(*a*). As all columns are assumed to be identical, the (0*kl*) reciprocal-lattice section will then correspond to the diffraction pattern of the projection of a single column down [100], each column having **a**-glide symmetry. The very shape of the columns requires displacements parallel to [010] and [001] of the monoclinic cell when columns are stacked together, these being $\pm\mathbf{b}/4$ and $\pm\mathbf{c}/4$, but possible displacements parallel to [100] are harder to define. The experimental observation that all maxima with $h = 3n$ are sharp suggests that these displacements must be integral multiples of **a**/3, **a**/6, ..., *etc.*, but more detailed information can be obtained from the non-space-group absences displayed by these sections. In particular, superposition of sections with $h = 6n$ only implies a true displacement of **a**/6, and the conditions $k + l = 4n$ for $h = 6n$ and $k + l = 4n + 2$ for $h = 6n + 3$ imply the presence of equivalent points at (0,0,0) and $(\frac{1}{4},\frac{1}{4},\frac{1}{6})$, (referred to monoclinic axes) irrespective of the structural variant present. The simplest interpretation is then one where each column in the structure is surrounded by neighbours stacked with a displacement of $+\mathbf{a}/6$ ($\mathbf{V}_1$) or $-\mathbf{a}/6$ ($\mathbf{V}_2$) in the [100] direction, and that any possible stacking sequences must involve one or other of these displacements.

Derivation of structural variants

With the above criteria, the various possible structures can then be enumerated in order of increasing complexity, by considering the different stacking sequences which can occur along each {011} plane in turn. These are given in Table 3, some of the simpler

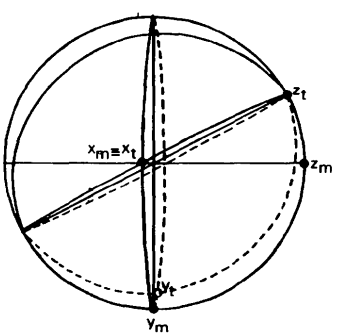

Fig. 4. Stereographic projection showing the mutual orientation of axial elements of monoclinic and triclinic structural variants of ganophyllite.

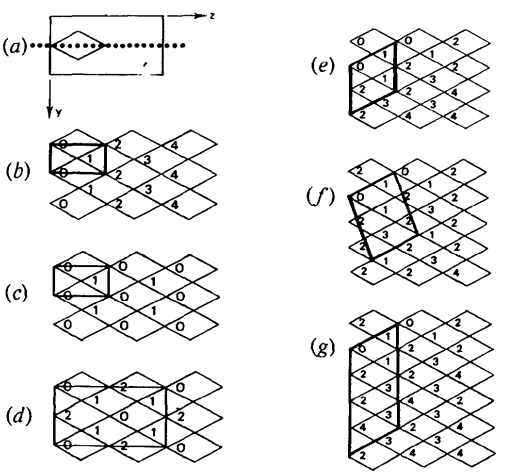

Fig. 5. Schematic illustration of possible structural variants of ganophyllite with the structural column concept. (*a*) Single column, (*b*)–(*d*) monoclinic structures, (*e*)–(*g*) triclinic structures. [Relative displacements of columns are indicated in multiples of **a**/6 from the (100) plane of the known monoclinic variant.]

Table 3. *Some of the simpler stacking sequences for structural columns in ganophyllite*

Stacking sequences along both {011} planes
Monoclinic
(1) $\mathbf{V}_1\mathbf{V}_1\mathbf{V}_1\mathbf{V}_1\mathbf{V}_1\mathbf{V}_1\mathbf{V}_1\mathbf{V}_1\ldots$
(2), (3) $\mathbf{V}_1\mathbf{V}_2\mathbf{V}_1\mathbf{V}_2\mathbf{V}_1\mathbf{V}_2\mathbf{V}_1\mathbf{V}_2\ldots$

Stacking sequences along each {011} plane
Triclinic
(4) $\mathbf{V}_1\mathbf{V}_2\mathbf{V}_1\mathbf{V}_2\mathbf{V}_1\mathbf{V}_2\mathbf{V}_1\mathbf{V}_2\ldots$ (011)
$\mathbf{V}_1\mathbf{V}_1\mathbf{V}_1\mathbf{V}_1\mathbf{V}_1\mathbf{V}_1\mathbf{V}_1\mathbf{V}_1\ldots$ (01$\bar{1}$)
(5) $\mathbf{V}_1\mathbf{V}_2\mathbf{V}_1\mathbf{V}_2\mathbf{V}_1\mathbf{V}_2\mathbf{V}_1\mathbf{V}_2\ldots$ (011)
$\mathbf{V}_1\mathbf{V}_1\mathbf{V}_2\mathbf{V}_1\mathbf{V}_1\mathbf{V}_2\mathbf{V}_1\mathbf{V}_1\ldots$ (01$\bar{1}$)
(6) $\mathbf{V}_1\mathbf{V}_2\mathbf{V}_1\mathbf{V}_2\mathbf{V}_1\mathbf{V}_2\mathbf{V}_1\mathbf{V}_2\ldots$ (011)
$\mathbf{V}_1\mathbf{V}_1\mathbf{V}_1\mathbf{V}_2\mathbf{V}_1\mathbf{V}_1\mathbf{V}_1\mathbf{V}_2\ldots$ (01$\bar{1}$)

structures being illustrated schematically in Fig. 5. For monoclinic variants, the stacking sequence along both planes must be the same: the simplest possible arrangement of this type is shown in Fig. 5(*b*), with constant $\mathbf{V}_1$ displacements. This will produce a monoclinic $A2/a$ structure, but with only one-half the cell dimensions and a different β value from those actually observed. Where alternate displacements of $\mathbf{V}_1$ and $\mathbf{V}_2$ are considered along each plane, two monoclinic arrangements can result, shown in Fig. 5(*c*) and (*d*). The first produces a cell of similar size to that of Fig. 5(*b*), but with the correct β angle, although losing the A lattice symmetry, whereas the second produces a larger unit cell corresponding to that observed experimentally. An intensity calculation for this second model then produces the theoretical reciprocal-lattice intensity variation illustrated in Fig. 6(*a*), giving good agreement with experiment.

If the condition that identical stacking sequences are employed along both fault planes is relaxed, triclinic structural variants will result. Fig. 5(*e*), (*f*), and (*g*) indicates this. In the situation shown in Fig. 5(*e*) the sequence is $\mathbf{V}_1\mathbf{V}_2\mathbf{V}_1\mathbf{V}_2\ldots$ along the (011) planes but $\mathbf{V}_1\mathbf{V}_1\mathbf{V}_1\mathbf{V}_1\ldots$ along (01$\bar{1}$), producing a small triclinic cell, or alternatively, a larger cell with the same [010] as the large monoclinic cell. In Fig. 5(*f*) the sequence along (011) is retained, but that along (01$\bar{1}$) is of the form $\mathbf{V}_1\mathbf{V}_1\mathbf{V}_2\mathbf{V}_1\mathbf{V}_1\mathbf{V}_2\ldots$, producing a larger triclinic cell, an extremely large cell being required if the monoclinic [010] axis direction is preserved. If the repeat distance of the (0$\bar{1}$1) sequence is increased by a further vector, to $\mathbf{V}_1\mathbf{V}_1\mathbf{V}_1\mathbf{V}_2\mathbf{V}_1\mathbf{V}_1\mathbf{V}_1\mathbf{V}_2\ldots$. (Fig. 5*g*) then the observed triclinic cell will result. Theoretical reciprocal-lattice intensity variations for this model (Fig. 6*b*) then show good agreement with experiment, their most striking feature being that apparent systematic absences on $h = 3n \pm 1$ sections for this structure are, in fact, merely systematically weak reflections.

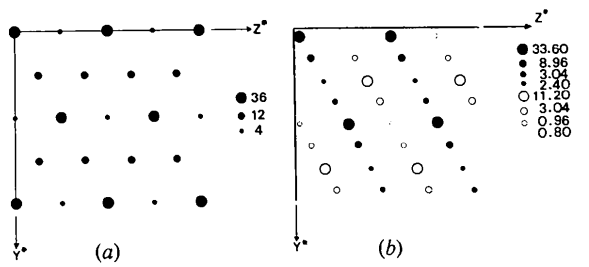

Fig. 6. Calculated reciprocal-lattice intensities for the ($1kl$) sections for the two structures observed (*a*) monoclinic structure, (*b*) triclinic structure. In each case the traces of the monoclinic y^* and z^* are indicated.

Conclusions

Although more complex than a one-dimensional treatment, the two-dimensional model of disorder in ganophyllite can explain all the observed features. In particular, the case of a crystal exhibiting the monoclinic and twinned triclinic structures, such as that in Fig. 2, can be represented as an intergrowth of monoclinic and triclinic domains, bounded by {011} planes, shown schematically in Fig. 7. From X-ray diffraction evidence, however, such domains must be relatively large, otherwise only very diffuse maxima would be observed on reciprocal-lattice sections with $b = 3n \pm 1$, and these sections would, in fact, consist of planes of diffuse scattering in reciprocal space.

Further, more complex structures than those described above can be derived by invoking more complicated stacking sequences along one or both of the {011} planes. An infinite number of structures can therefore exist for ganophyllite, and although the concept of identical layers cannot be applied to the structure, the variation observed is nevertheless akin to a form of polytypism, as the experimental observations can be accounted for quite satisfactorily by a model involving differing stacking sequences of identical structural units.

The complexity of the structural variants observed in

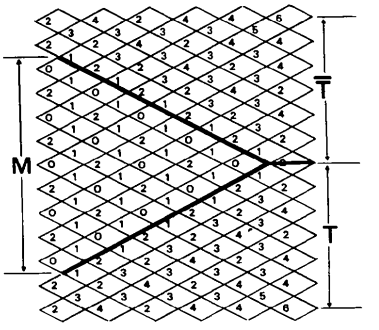

Fig. 7. Schematic illustration of the intergrowth of monoclinic (M) and twinned triclinic (T and $\bar{T}$) structures, producing a wedge-shaped monoclinic domain. (Relative displacements are indicated as in Fig. 5.)

ganophyllite raises several interesting questions, the most important being the apparent absence of any of the simpler structures described above. This would suggest that some form of ordering scheme exists, giving rise to relatively long-range structural control. Variation of structural form with chemical composition has long been known in micas and other layered silicates (see, for example, Radoslovich, 1963) and the complex composition of ganophyllite, given by Smith & Frondel (1968) as $(K_{1\cdot87}Na_{2\cdot29})(Mg_{0\cdot16}Ca_{0\cdot65}Pb_{0\cdot03}Mn_{16\cdot14}Fe_{0\cdot36})O_{52\cdot6}(OH)_{35\cdot4}$ appears to imply a capacity for chemical substitution. Whether such a variation could be detected by conventional electron-microprobe methods is a matter of speculation, but compositional differences have been investigated in this way in zussmanite (Jefferson, 1976) and the detection of similar chemical substitution in chloritoid (Crawford, Jefferson & Thomas, 1978) by energy-dispersive analysis in the electron microscope, suggests a possible avenue of further investigation.

References

COCHRAN, W. & HOWELLS, E. R. (1954). *Acta Cryst.* **7**, 412–415.

CRAWFORD, E. S., JEFFERSON, D. A. & THOMAS, J. M. (1977). *Acta Cryst.* A**33**, 548–553.

CRAWFORD, E. S., JEFFERSON, D. A. & THOMAS, J. M. (1978). In preparation.

EGGLETON, R. A. (1972). *Mineral. Mag.* **38**, 693–711.

EGGLETON, R. A. & BAILEY, S. W. (1965). *Clays Clay Miner.* **13**, 49–63.

HAMBERG, A. (1890). *Geol. Foeren. Stockholm. Foerh.* **12**, 586–598.

JEFFERSON, D. A. (1976). *Am. Mineral.* **61**, 470–483.

JEFFERSON, D. A. & BOWN, M. G. (1973). *Nature (London) Phys. Sci.* **245**, 43–44.

LOPES-VIEIRA, A. & ZUSSMAN, J. (1969). *Mineral. Mag.* **37**, 49–60.

RADOSLOVICH, E. W. (1963). *Am. Mineral.* **48**, 348–367.

SMITH, M. L. & FRONDEL, C. (1968). *Mineral. Mag.* **36**, 893–913.

Acta Cryst. (1978), A**34**, 497–500

X-ray Measurement of the Root-Mean-Square Displacement of the Atoms in Cadmium Single Crystals

BY ELISABETH ROSSMANITH

Mineralogisch-Petrographisches Institut der Universität Hamburg, 2000 *Hamburg* 13, *Grindelallee* 48, *Federal Republic of Germany*

(*Received* 18 *October* 1977; *accepted* 9 *February* 1978)

The root-mean-square displacements u_a and u_c of the cadmium atoms in single crystals in the **a** and **c** directions, respectively, were determined by the use of Bragg intensities obtained with Mo $K\alpha$ radiation. The results [$u_a = 0\cdot121$ (1), $u_c = 0\cdot196$ (1) Å] are compared with other X-ray measurements.

Introduction

As stated in Rossmanith (1977) (R-77 hereinafter) the thermal parameters obtained by the use of least-squares fits of observed and calculated structure factors are in satisfactory agreement with values obtained by other methods, if (*a*) the substances consist of heavy atoms and are highly symmetrical, so reducing the six thermal parameters to one or two independent parameters, and if (*b*) the corrections for absorption, extinction and TDS are properly made.

It was shown in R-77 that in the case of Zn, in which there is high extinction, the results obtained for u_a and u_c, the root-mean-square displacements in the **a** and **c** directions of the crystal, were in good agreement with those obtained by Skelton & Katz (1968), measured in the temperature range 4·85 to 600 K.

This encouraged the author to determine the root-mean-square displacement of Cd with the help of least-squares procedures. For Cd, where extinction is severe, mainly because of the high atomic number of Cd, again it can be shown that the values of the thermal parameters are strongly affected by extinction correction.

Experimental

Two spherical Cd single crystals (99·9999% Cd) were supplied by Guse (1971). The experimental procedure is very similar to that described in R-77. The main features of the measurement are shown in Table 1.

All reflexions were measured four times. For each reflexion the error in the measured intensity, ΔI, was calculated, taking into account the variance from